Nuclear Instruments and Methods in Physics Research B 306 (2013) 158–164

Contents lists available at SciVerse ScienceDirect

Nuclear Instruments and Methods in Physics Research B

journal homepage: www.elsevier.com/locate/nimb

Energy deposition in small-scale targets of liquid water using the very low energy electromagnetic physics processes of the Geant4 toolkit

S. Incerti [a,*], C. Champion [a], H.N. Tran [a], M. Karamitros [b], M. Bernal [b], Z. Francis [c], V. Ivanchenko [d], A. Mantero [e], Members of the Geant4-DNA collaboration

[a] Université Bordeaux 1, CNRS/IN2P3, Centre d'Etudes Nucléaires de Bordeaux Gradignan, CENBG, Gradignan, France
[b] Instituto de Física Gleb Wataghin, Universidade Estadual de Campinas, SP, Brazil
[c] Université Saint Joseph, Science Faculty, Department of Physics, Beirut, Lebanon
[d] Ecoanalytica, 119899 Moscow, Russia
[e] Istituto Nazionale di Fisica Nucleare, sez. di Genova, Genova, Italy

ARTICLE INFO

Article history:
Received 21 July 2012
Received in revised form 18 October 2012
Accepted 10 December 2012
Available online 24 January 2013

Keywords:
Monte Carlo
Geant4
Geant4-DNA
Microdosimetry
Electromagnetic interactions

ABSTRACT

In the perspective of building an open source simulation platform dedicated to the modelling of early biological molecular damages due to ionising radiation at the DNA scale, the general-purpose Geant4 Monte Carlo simulation toolkit has been recently extended with specific very low energy electromagnetic physics processes for liquid water medium. These processes – also called "Geant4-DNA" processes – simulate the physical interactions induced by electrons, hydrogen and helium atoms of different charge states. The present work reports on the energy deposit distributions obtained for incident electrons, protons and alpha particles in nanometre-size volumes comparable to those present in the genetic material of mammalian cells. The frequency distributions of the energy deposition obtained for three typical geometries of nanometre-size cylindrical targets placed in a spherical phantom are found to be in reasonable agreement with prior works. Furthermore, we present a combination of the Geant4-DNA processes with a simplified geometrical model of a cellular nucleus allowing the evaluation of energy deposits in volumes of biological interest.

1. Introduction

The Geant4-DNA project [1] was initiated in 2001 by the European Space Agency in the perspective of building an open source simulation platform dedicated to the modelling of early biological molecular damages induced by ionising radiation at the DNA scale. This platform is part of the general-purpose Geant4 Monte Carlo simulation toolkit [2,3]. Geant4 is used for large scale simulation of the Large Hadron Collider experiments and other high energy physics applications, for space science, for medical physics and for many other applications. It is developed by an international collaboration and released as open source software. In this context, Geant4 currently proposes to users a full set of processes and models – the so called "Geant4-DNA" processes and models – for the simulation of physical interactions of electrons, hydrogen (including the H^0 and H^+ charge states) and helium atoms (including the He^0, He^+ and He^{2+} charge states) in liquid water down to very low energies (∼eV for electrons and ∼1 keV/amu for ions). The cross sections available in the Geant4-DNA models have been recently compared to a large collection of experimental cross sections in water vapour [4]. Furthermore, stopping powers as well as ranges derived from Geant4-DNA simulations have been compared to international recommendations for the liquid phase [5]. In parallel, additional Geant4-DNA classes are being developed for the simulation of water radiolysis under irradiation, taking into account the production, diffusion and chemical interactions of molecular species and oxidative radicals [6]. Indeed, it is nowadays well recognised that the simulation of both physics and physico–chemistry/chemistry processes occurring during the irradiation of liquid water in small geometries are required for the modelling of early radiation effects at the scale of DNA (see for example Friedland et al. [7]).

First attempts to compare Geant4-DNA physics modelling capabilities at the nanometre scale with another Monte Carlo code developed at the Physikalisch-Technische Bundesanstalt in Germany have been recently published [8,9]. These studies simulated the transport of pencil beams of monoenergetic particles inside a cylindrical volume with dimensions equivalent either to a DNA segment or to a nucleosome. They pointed out differences in terms of nanodosimetric parameters of track structure originating from different cross section models used in both codes. Recently, the

* Corresponding author. Address: Université Bordeaux 1, CNRS/IN2P3, Centre d'Etudes Nucléaires de Bordeaux Gradignan, CENBG, Chemin du Solarium, BP120, 33175 Gradignan, France. Tel.: +33 5 57 12 08 89; fax: +33 5 57 12 08 01.
E-mail address: incerti@cenbg.in2p3.fr (S. Incerti).

0168-583X/$ - see front matter © 2013 Elsevier B.V. All rights reserved.
http://dx.doi.org/10.1016/j.nimb.2012.12.054

study by Bernal et al. [10] explained the predicted invariance of total direct DNA strand break yields as a function of the LET of the incident ionising particles, using exclusively the Geant4-DNA physics processes. Track structures were combined with an externally implemented geometrical model of chromatin fibres containing 5.4×10^8 nanometre-size volumes corresponding to base pairs of DNA.

In the present work, we present the use of Geant4-DNA physics processes in nanometre-size targets fully implemented in a single Geant4 application. The frequencies of the deposited energy per incident particle are presented in a highly voxellized geometrical target in order to evaluate the energy depositions induced by electrons, protons and alpha particles in nanometre-size cylindrical volumes comparable to DNA segments, nucleosomes and elements of the chromatin fibre. These frequencies are compared to existing works. Finally, a Geant4 application based on the combination of Geant4-DNA processes with a simplified geometrical model of a cellular nucleus is presented. This nucleus is built from a highly voxellized target containing cylindrical volumes which are filled with a geometrical model of chromatin fibre in the B-DNA conformation. Frequencies of the deposited energy per incident particle are presented.

2. Methods

2.1. Geant4-DNA very low energy processes

The results presented in this work have been obtained using the physical processes available in the Geant4-DNA extension of the Geant4 toolkit. These processes have been previously described in detail by Incerti et al. [4]. They are applicable to electrons and hydrogen and helium atoms of different charge states (H^0, H^+) and (He^0, He^+, He^{2+}) respectively, and to C^{6+}, N^{7+}, O^{8+} and Fe^{26+} ions, in liquid water (density equals to 1 g cm^{-3}) [11]. These physical processes include ionisation (for all particles), electronic excitation (for electrons, protons, hydrogen atoms and alpha particles including their different charge states), charge exchange (for hydrogen and helium atoms with the above-mentioned charge states), and, for electrons, elastic scattering, vibrational excitation and molecular attachment. Electron interactions cover the 7.4 eV–1 MeV energy range, whereas proton and hydrogen interactions are simulated from 100 eV to 100 MeV while helium ions of different charged states are followed from 1 keV up to 400 MeV. By default, electrons are tracked down to 7.4 eV. The production of Auger electrons after oxygen K-shell ionizations is included in the results presented here and is available to users since the last public release of the Geant4 toolkit, thanks to recent developments included in Geant4 [12] that allow to simulate atomic de-excitation effects in both categories of the Geant4 electromagnetic physics processes (the so-called "standard" and the "low energy" categories).

2.2. Voxellized phantom containing nanometre-size geometries

In a perspective of simulating the elementary energy depositions on DNA structures in a simplified model of a biological cell nucleus using Geant4-DNA processes, a spherical 3D voxellized phantom containing liquid water was implemented directly in a Geant4 simulation application. We followed the procedure that we initially proposed in the Geant4 "microbeam" example for targeted cellular irradiation [13], which includes a full cellular realistic phantom obtained from confocal microscopy. The phantom (1 μm diameter) used in this work is filled in with liquid water and it is placed in vacuum. All adjacent parallelepiped voxels of the cellular phantom have been replaced by spherical voxels, immersed in liquid water. Each spherical voxel is filled with liquid water. A cylindrical target, also filled with liquid water, is placed at the centre of each spherical voxel whose radius is equal to the half diagonal of the cylindrical target. Each cylinder is randomly oriented in space. As a result, we build a full phantom containing cylindrical targets made of liquid water fully randomly oriented and immersed in liquid water. Using this phantom approach, cylindrical targets never overlap with neighbours since they are fully contained in adjacent spherical voxels. Cylindrical targets have dimensions (diameter × height) of genetic units of mammalian cells originally proposed by Charlton and colleagues [14–17], namely, 2 nm × 2 nm, 10 nm × 5 nm and 25 nm × 25 nm for DNA segments, nucleosomes and chromatin fibres, respectively.

2.3. Irradiation conditions

Mono-energetic incident radiation was shot in the direction of the centre of the spherical phantom from points randomly placed on a virtual spherical surface tangent to the spherical voxels located at the periphery of the phantom. Doing this, the thickness of liquid water encountered by incoming particles is constant. Besides, the random placement of the emission point on the virtual sphere ensures random crossing of cylinders from one incident particle to the next one. For comparison, random shooting of incident particles with an isotropic direction around the phantom was also considered. Both irradiation configurations are illustrated in Fig. 1.

2.4. Particle tracking settings

In order to compare the energy deposition patterns obtained from single tracks with the earlier works of Nikjoo et al. [17] and by Cucinotta et al. [16], we follow each primary as well as every secondary electron down to a pre-defined energy cut-off of 10 eV. The tracking of electrons with lower kinetic energies (for e.g. secondary electrons produced from ionisation) is stopped. Their kinetic energy is then fully released into the liquid water medium. In the case of incident ions, stationary regime was maintained by setting after each simulation step the kinetic energy of the particle to its incident value in all energy loss processes, excitation and ionisation, as proposed by Charlton et al. [15]: under these conditions, the charge exchange process has been obviously not considered.

2.5. A simplified geometrical model of cell nucleus

A simple geometrical model of a biological cell nucleus was constructed from the phantom containing randomly oriented cylinder volumes presented previously. Each cylinder was filled with a geometrical model of a segment of chromatin fibre. Following a first attempt (see Ref. [1]), the segment of chromatin fibre was modelled in a Geant4 application thanks to the original work of Bernal and Liendo [18]. This chromatin fibre model includes geometrical volumes describing nucleosomes, DNA loops and bases. The DNA double helix consists in a series of slices in the B-DNA conformation, each of them including two phosphodiester groups bound by a complementary base pair. Nitrogenous bases pairs are represented by 0.33 nm-thick cylindrical shells. Each slice is rotated from its neighbour in order to build a full double helix loop of 100 bp. Nucleosomes are modelled as a cylindrical histones surrounded by two DNA loops. Each segment of the 30-nm chromatin fibre contains a total of 3600 DNA base pairs. All components are assumed to contain liquid water. The whole nucleus considered in this work is taken as a virtual sphere of radius 7.5 μm, in reasonable agreement with recently measured several HaCat cell nucleus thicknesses using confocal microscopy imaging [19]. This geometrical model contains about 1.67×10^6 randomly oriented cylinders,

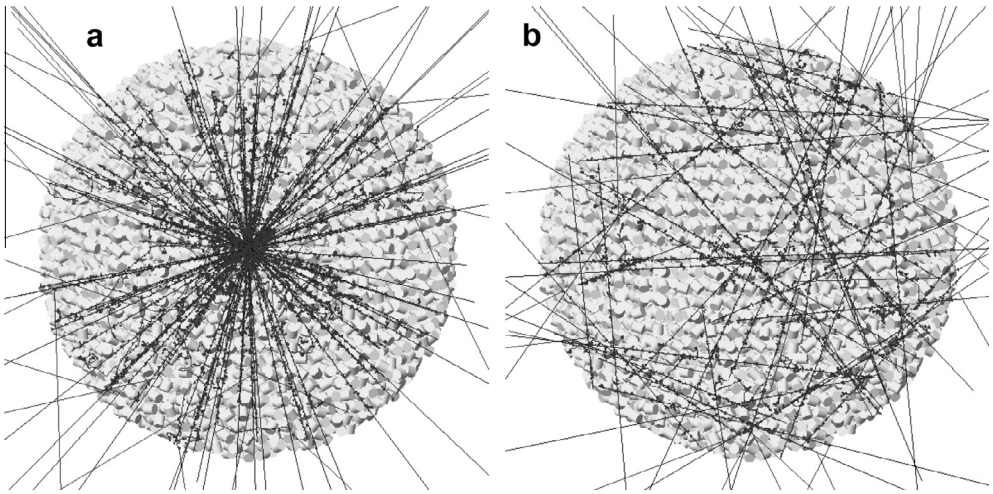

Fig. 1. Example of Geant4 visualisation of the 1 μm diameter liquid water spherical phantom placed in vacuum and containing 10,552 cylindrical targets of dimensions 25 nm (d) × 25 nm (h). These targets are randomly oriented in space and correspond to chromatin fibre units. On this figure, the phantom is irradiated by 50 incident protons of 2 MeV; Panel (a) shows a centred irradiation while panel (b) shows a random isotropic irradiation. Proton tracks overlap graphically but they are fully treated as single track events. Outgoing protons leave the phantom and penetrate into vacuum; none of the escaping particles interact in the vacuum region.

for a total of 6×10^9 DNA base pairs, corresponding to the genomic content of a human cell in its interphase [20].

3. Results and discussion

3.1. Frequency distributions of energy deposition f(>E) in nanometric cylinders

Frequency distributions of energy deposition in the cylindrical targets were calculated for each single incident particle and were averaged over the total number of incident particles shot onto the phantom. They have been calculated for incident electrons, protons and alpha particles and for the three above-cited cylindrical targets. Results are presented per target cylinder and per Gray deposited in the virtual sphere containing the target cylinders. We here report results for 1 keV electrons, 2 MeV protons and 1.2 MeV alpha particles, the latter being used for comparison with previous predictions [21]. Besides, the accuracy of the sampling was checked by verifying that the ratio of irradiated volumes (sampled cylindrical targets volume over virtual sphere volume) was less than a few percent different from the dose ratio (sampled cylindrical targets dose over virtual sphere dose) as proposed by Charlton et al. [14].

Fig. 2 shows the frequency of energy distribution $f(>E)$ for 1 keV electrons in two target cylinder geometries: 25 nm × 25 nm (top curves) and 2 nm × 2 nm (bottom curves). The total numbers of cylinders and their corresponding densities are given in Table 1. Note that these density values are the maximum reachable densities of cylinders using this geometrical implementation (based on a phantom approach), which avoids geometrical overlapping of cylinders. For each geometry, we investigated the effect of shooting incident electrons either towards the centre of the virtual sphere (labelled "centred") or with an isotropic distribution (labelled "random"). The Geant4-DNA results are compared to the MOCA8B Monte Carlo calculations shown in Nikjoo et al. [17]. The global tendency of the frequency distribution for the energy deposition is reproduced although disagreements are observed at low and high energies.

Fig. 3 shows the frequency of the energy deposit distribution $f(>E)$ for 2 MeV protons for three target cylinder sizes: 25 nm × 25 nm (top curves), 10 nm × 5 nm (middle curves) and 2 nm × 2 nm (bottom curves). These frequencies are compared to

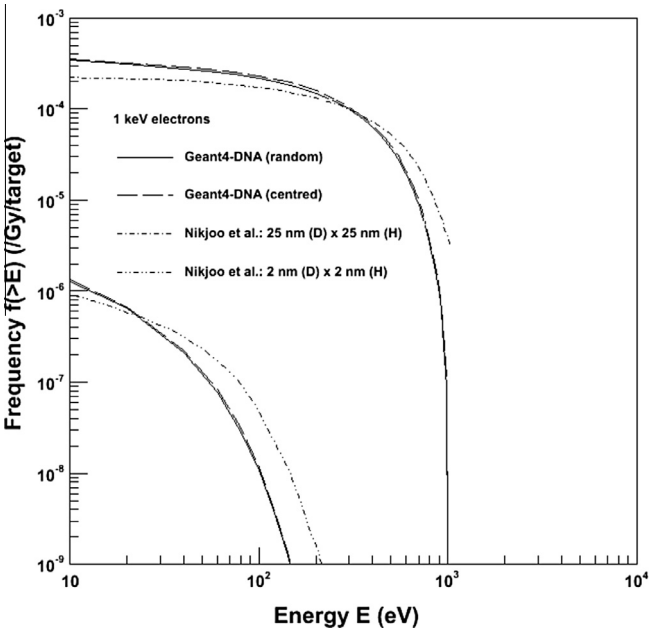

Fig. 2. Frequency distributions of the energy deposition $f(>E)$ per cylinder target and per Gy deposited in the virtual sphere and obtained with 1 keV incident electrons for two geometries of the cylinders (top curves: 25 nm (D) × 25 nm (H), bottom curves: 2 nm (D) × 2 nm (H)). Electrons were shot either in the direction of the centre of the virtual sphere ("centred") or randomly in the 3D space ("random"). For comparison purpose, data published by Nikjoo et al. [17] are also shown.

those obtained using the MOCA14 code and reported in [16]. All curves have the same trend as a function of deposited energy. Furthermore, let us note that the simulated distributions are very similar to those of Fig. 2, which is due to the fact that 2 MeV protons and 1 keV electrons have comparable velocities. Electrons and protons travelling through a gas at the same speed have similar ionisation cross sections when protons energy is above about 0.5 MeV [22]. We still observe that the obtained frequencies are in agreement with those of Cucinotta et al. [16], in particular in the low-energy region, and discrepancies may be seen between the two codes in the high-energy domain, up to one order of magnitude for the 10 nm × 5 nm geometrical cylinder case.

Table 1
The dimensions of the cylindrical targets, the radius of the voxellized phantom, the number of spherical voxels within the phantom (which is equal to the number of cylindrical targets) and the corresponding densities are given. The radius of the phantom for the 2 × 2 cylinder geometry was reduced to 150 nm in order to limit the number of voxels in computer memory during the Geant4 simulations.

Dimensions of the cylinders diameter × height (nm × nm)	Radius of the phantom (nm)	Number of spherical voxels or cylinders in the phantom	Density of the spherical voxels or cylinders in the phantom (nm^{-3})
25 × 25	500	10552	2.1×10^{-5}
10 × 5	500	362493	7.0×10^{-4}
2 × 2	150	606984	4.3×10^{-2}

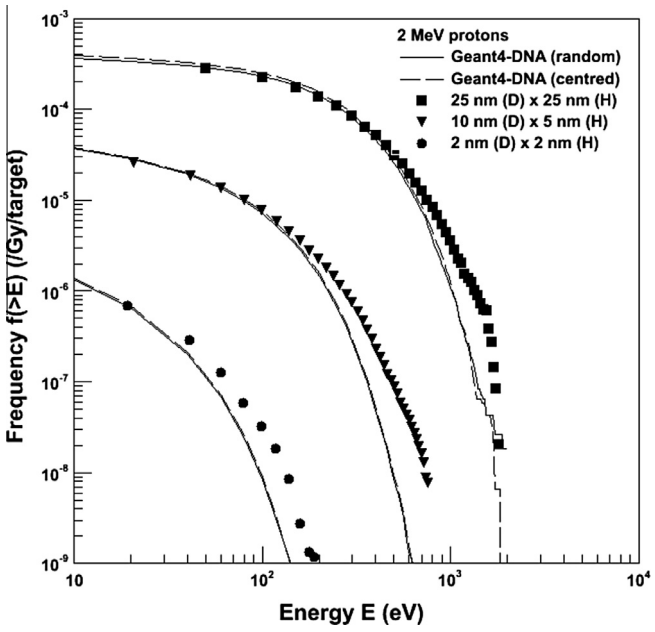

Fig. 3. Frequency distributions of the energy deposition $f(>E)$ per cylinder target and per Gy deposited in the virtual sphere, obtained with 2 MeV incident protons for the three cylinder sizes. Cylinder diameter and height values are indicated. Protons were shot either in the direction of the centre of the virtual sphere (“centred”) or randomly in the 3D space (“random”). For comparison purpose, data of Charlton et al. reported by Cucinotta et al. [16] for the same geometries are indicated.

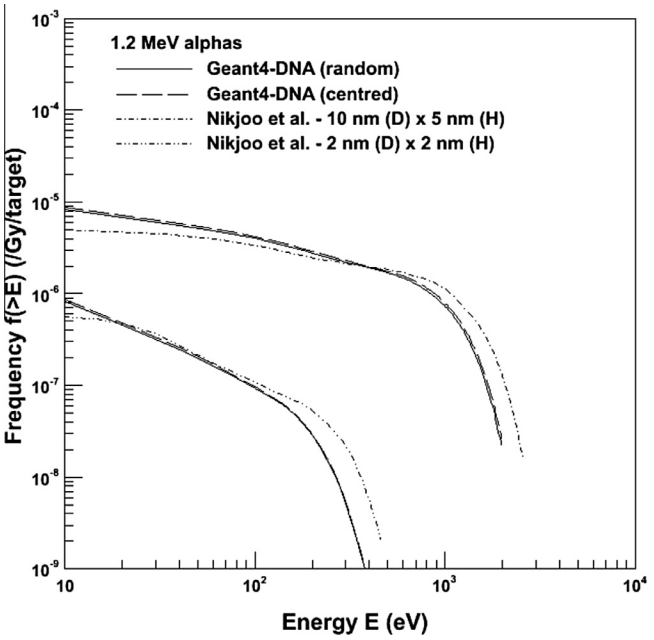

Fig. 4. Frequency distributions of energy deposition $f(>E)$ per cylinder target and per Gy deposited in the virtual sphere, obtained with 1.2 MeV incident alpha particles for two cylinder sizes (top curves: 10 nm (D) × 5 nm (H), bottom curves: 2 nm (D) × 2 nm (H)). Cylinder diameter and height values are indicated. Alpha particles were shot either in the direction of the centre of the virtual sphere (“centred”) or randomly in the 3D space (“random”). The Geant4-DNA results are compared to the work of Nikjoo et al. [21].

Finally, Fig. 4 shows the frequencies obtained for 1.2 MeV alpha particles in two cylinder geometries (top curves: 25 nm × 25 nm , bottom curves: 2 nm × 2 nm). They are compared to the results of Nikjoo and Lindborg [21]. Here again, the tendency is well reproduced and differences appear at lowest and highest energy deposits.

Figs. 2–4 show trends in nanometer-size volumes similar to the corresponding reference works. We have verified that the method of shooting incident particles on the cylinder targets (“centred” or “random”) has no significant effect on the shape of the frequencies distributions. In addition, varying the number of cylindrical targets did not impact the results. The discrepancies observed for large energy deposits between the Geant4-DNA results and the MOCA results origin mainly from the different physics models available in the codes. In this context, let us remind here that the electron Geant4-DNA inelastic models are based on the dielectric formalism [4] while the MOCA models derive from various sources (see for e.g. [23]: ionisation data for inner shell: Drawin formula and fit to the data of Glupe and Mehlhorn, ionisation data for outer shell: Tan et al. data and own analysis, excitation data from various sources and own analysis, etc.). These differences in terms of differential and total ionising cross sections lead to macroscopic discrepancies between the two codes such as the stopping power which is found lower in the Geant4-DNA approach in comparison to the MOCA’s values (for more details we refer the reader to Fig. 7 of [4] and Fig. 5 of [23]). In particular, for 1 keV incident electrons, the Geant4-DNA stopping power is about 40% lower than the MOCA’s value what undoubtedly affects the energy deposition pattern. Thus, we clearly observe from Fig. 2 that the low-energy deposits are more abundant in our simulation whereas the high-energy deposits are lesser. Finally, Figs. 3 and 4 report the proton and alpha particles results. In both cases we obtain the same tendency than that observed for electrons.

3.2. Frequency distributions of energy deposition in the simplified nucleus model

For incident protons, we extracted the frequency distributions of energy deposition $f(>E)$ per incident proton (so-called “event”) in target volumes corresponding to phosphodiester groups (so-called “target”). For this simulation, we activated all Geant4-DNA physics processes, such as charge exchange for protons, and the kinetic energy of the incident protons was not fixed to its incident value as before. The phosphodiester groups are shaped as prisms with a thickness of 0.33 nm, an inner radius of 0.5 nm and an outer radius of 1.185 nm, with a 73 degrees angular aperture [18]. The first energy excitation level of liquid water in the Geant4-DNA models is set to 8.22 eV and the first ionisation level to 10.79 eV [4]. Then, for 2 MeV protons emitted in the direction of the nucleus centre, the frequency of the energy deposits above 8.22 eV per target and per Gray deposited in the virtual sphere is equal to $(8.05 \pm 0.05) \times 10^{-8}$. If we now assume that an energy deposit of 8.22 eV is sufficient to induce a direct DNA single strand break (so-called “SSB”) in the DNA loops, then the resulting number of

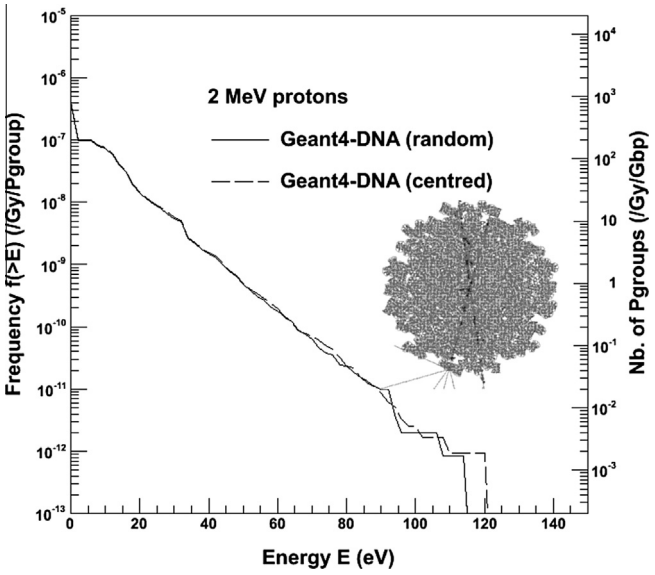

Fig. 5. Frequency distributions of energy deposition $f(>E)$ in the simplified nucleus geometrical model per phosphodiester group and per Gy deposited in the virtual sphere, obtained with 2 MeV incident protons for a total absorbed dose of 100 Gy. Protons were shot either in the direction of the centre of the virtual sphere ("centred") or randomly in the 3D space ("random"). The right axis indicates the number of phosphodiester groups per Gray and per Gbp which have received a total energy deposit above the energy threshold "Energy". A superimposition of two proton tracks hitting the simplified nucleus model is shown.

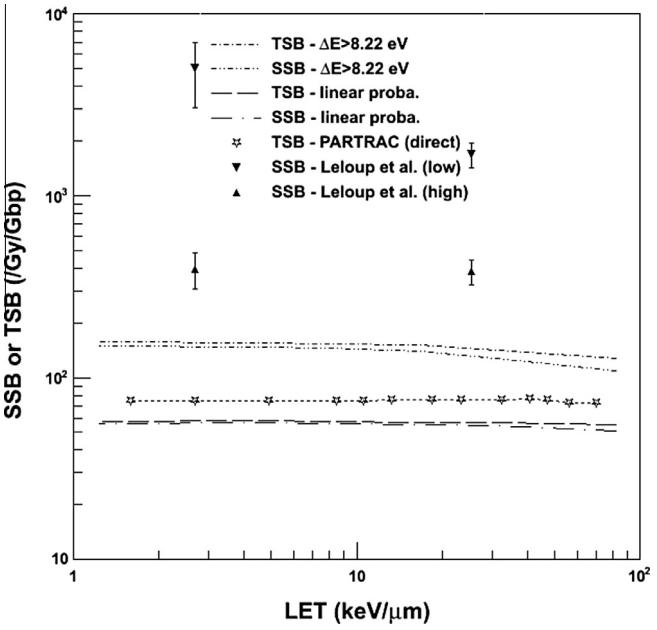

Fig. 6. Estimation of direct single (SSB) and total strand breaks (TSB) obtained for several incident proton LET values. Accounting for direct SSBs was performed assuming that either a total energy deposit above 8.22 eV is required in a target volume ("$\Delta E > 8.22$ eV") or that the probability to induce a direct SSB depends linearly on the deposited energy in the target volume ("linear proba.") as proposed by Friedland et al. [25]. The simulated total direct yields from Friedland et al. [20] are shown (star symbols, which are joined by a dashed line for better visibility). Experimental data on DNA plasmids at low and high scavenger concentrations by Leloup et al. [27] are also indicated.

SSB is 161 ± 1 SSBs per Gray per Giga base pair (Gbp). If the energy deposit threshold is increased up to 10.79 eV instead of 8.22 eV, the frequency above this threshold reaches $(6.70 \pm 0.05) \times 10^{-8}$ and the predicted number of SSBs reaches 134 ± 1 SSBs per Gray per Gbp. These estimations have been obtained by accumulating about 100 Gy into the virtual sphere. Fig. 5 shows both the frequency distributions of energy deposition $f(>E)$ (per Gray and per phosphodiester group, left vertical axis) and the number of phosphodiester groups in the geometrical model receiving more than the energy threshold E (per Gray and per Gbp, right vertical axis). The two curves were obtained for protons emitted either in the direction of the centre or isotropically in space ("centred" or "random"). Here again, similar profiles are observed in both cases and we observe a slight increase of the frequency in the first bin (<2 eV) which is linked to the account of the vibrational excitations induced by the low-energy electrons [24]. For illustration, we also superimposed a Geant4 visualisation of two proton tracks penetrating into the simplified nucleus model.

As an alternative to the method described above, the extraction of direct SSBs can be calculated per incident particle in the nucleus geometrical model directly during the tracking of particles by assuming that a total energy deposit in a phosphodiester group (target) volume above a given threshold, such as 8.22 eV (or 10.79 eV), can induce a SSB. Besides, Friedland et al. [25] proposed that the probability of creating a SSB depends on the value of the deposited energy in the target volume: this probability is taken as linear from 0 to 1 between 5 eV and 37.5 eV and equal to 1 above 37.5 eV. Both approaches can be tested with the Geant4 simplified geometrical model of the nucleus. From the localization of SSBs, it is also possible to define double stand breaks (DSBs) along DNA loops. We assume here that a maximum distance of 10 bp separating two SSBs on opposite DNA strands is required to produce a single DSB. We tested both hypotheses to create a single strand break: either an individual target should receive at least a total energy deposit of 8.22 eV ("$\Delta E > 8.22$ eV" label) – as done in our previous work [10] – or the probability to induce a single strand break depends linearly on the value of the total energy deposit as proposed by Friedland et al. [25] ("linear proba." label). These estimations were obtained by shooting protons in the direction of the centre of the cell. Fig. 6 shows the numbers of single and total strand breaks (equals to SSB + 2 × DSB and labelled as "TSB") per Gray and per Giga base pair (Gbp) as a function of proton LET calculated at the centre of the nucleus. Complex damages were not considered in this work. For comparison purpose, total direct strand break estimations shown in Fig. 2 of the work of Friedland et al. [20] are also indicated, joined with a dashed line for better visibility. Errors are calculated as the statistical standard deviation of the mean and have been obtained for a total of about 100 Gy deposited in the virtual sphere; they are of the order of a few percent at maximum, for the number of DSBs calculated using the PARTRAC's method. In the simulated LET range, there is no strong dependence of the number of total strand breaks with the projectile's LET as previously described in [10] where an external geometrical model of chromatin fibres was used. It can be observed that these estimations depend strongly on the method used to account for a direct SSB (total deposit above a given threshold or linear probability to induce a direct SSB). In addition, it was recently found by Bernal et al. [26] that the strand break yield also depends on the geometrical description of the DNA configuration. The A-, B- and Z-DNA conformations have been studied in a geometrical assembly of chromatin fibres and it was found that the total direct strand break yield is determined by the phosphodiester group volume in each DNA configuration. This behavior is due to the quasi-constant number of inelastic events per unit absorbed dose for ion beams and that the site-hit probability is determined by the target volume. It is important to stress out that the absolute numbers of TSBs obtained using Geant4-DNA differ from the ones simulated by PARTRAC since the geometrical volumes describing phosphodiester groups in PARTRAC simulations are larger than

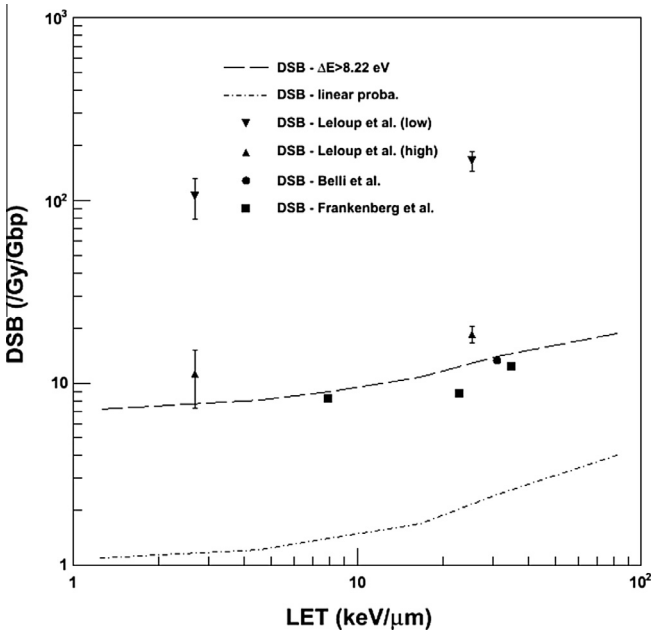

Fig. 7. Estimation of direct double strand breaks (DSBs) obtained for several incident proton LET values. Accounting for direct DSBs was performed assuming that two direct SSBs must be located on opposite strands and be distant by less than 10 bp. Experimental data on DNA plasmids at low and high scavenger concentrations by Leloup et al. [27] are also shown, as well as data on V79 cells by Belli et al. [28] and data on human skin fibroblasts by Frankenberg et al. [29].

the volume of the phosphodiester groups used in this work. For further comparison, an interesting perspective to this work could be to implement an alternative Geant4 geometrical model of B-DNA with dimensions similar to the ones used in PARTRAC. Experimental data on direct DNA damages from proton irradiation are not common. We report in Fig. 6 the data obtained by Leloup et al. [27] on plasmid DNA for high and low scavenger concentrations. Data obtained for the high concentration are expected to be closer to direct effects, although they still deviate significantly from Geant4-DNA and PARTRAC predictions. These data do not seem to depend strongly on the projectile's LET. Finally, we show in Fig. 7 double-stand break (DSB) estimations as a function of LET, which have been computed using both methods for SSB accounting (constant energy threshold or linear probability). Again, a strong dependence on the method to account for a SSB is observed. Simulations show an increase of the direct DSB yields as a function of LET, as we already reported [10]. Experimental data on plasmid DNA by Leloup et al. [27] for low and high scavenger concentrations, by Belli et al. on V79 cells [28] and by Frankenberg et al. on human skin fibroblasts [29] are also shown. The scavenging effect is clearly seen from the data by Leloup et al., where the high scavenger concentration data get closer to the simulated results, while the two other sets of experimental do not allow the distinction between direct and non-direct DSB yields. The results simulated using the linear probability method deviate the most from these experimental data.

4. Conclusions

In this work, we have used the Geant4-DNA physical processes of the Geant4 toolkit for the simulation of energy deposition by ionising radiation in nanometer size volumes. The frequency of the energy distributions were computed in a highly voxellized sphere containing nanometer size cylindrical targets compatible with genetic material units dimensions. This voxellized sphere has been fully implemented in a single Geant4 application. Using this integrated geometrical scoring, the energy deposition distributions show the same trend as previous works for electrons, protons and alphas but highlight differences in particular for the largest energy deposits. Finally, these cylinders were filled with a chromatin fibre model corresponding to the B-DNA conformation. With a total number of 6×10^9 bp, we estimated the production of direct single and double DNA strand breaks from incident protons in the 0.5–50 MeV range. The method selected to account for the production of a single strand break significantly impacts on the simulated results.

This work illustrates customizable features of the Geant4-DNA extension, such as the usage of a variety of physics processes in liquid water and the possibility to track particles and score physical energy deposition events in detailed user-defined geometries down to the nanometre scale, in a single Geant4 user application. Examples of energy deposition frequencies have then been here reported and compared with existing predictions provided by the well-known MOCA code. Thus, for electrons and light ions similar tendencies have been observed with nevertheless slight differences which are connected to the different approaches used by the Geant4-DNA and MOCA codes for describing the underlying physics involved in the particle tracking.

Acknowledgements

The Geant4-DNA project received funding from the French Agence Nationale de la Recherche contract number ANR-09-BLAN-0135-01 and from the European Space Agency BioRad Project under contract number AO6041-22712/09/NL/AT. It was also supported in part by the RFBR 09-02-91065 grant and the CNRS PICS-4865 grant. The Région Aquitaine, France, funded the computing farm used in this work through the RESEARCH project. M. Bernal thanks the FAEPEX fund, UNICAMP, and the FAPESP foundation (FAPESP 2011/51594-2), both in Brazil, for financing his research activities. This work has been developed as a part of the activities planned in the Programme de Coopération ECOS-*Sud* A09E04.

References

[1] S. Incerti, G. Baldacchino, M. Bernal, R. Capra, C. Champion, Z. Francis, P. Guèye, A. Mantero, B. Mascialino, P. Moretto, P. Nieminen, C. Villagrasa, C. Zacharatou, The Geant4-DNA project, Int. J. Model. Simul. Sci. Comp. 01 (2010) 157.

[2] S. Agostinelli, J. Allison, K. Amako, J. Apostolakis, H. Araujo, P. Arce, M. Asai, D. Axen, S. Banerjee, G. Barrand, F. Behner, L. Bellagamba, J. Boudreau, L. Broglia, A. Brunengo, H. Burkhardt, S. Chauvie, J. Chuma, R. Chytracek, G. Cooperman, G. Cosmo, P. Degtyarenko, A. Dell'Acqua, G. Depaola, D. Dietrich, R. Enami, A. Feliciello, C. Ferguson, H. Fesefeldt, G. Folger, F. Foppiano, A. Forti, S. Garelli, S. Giani, R. Giannitrapani, D. Gibin, J.J. Gómez Cadenas, I. González, G. Gracia Abril, G. Greeniaus, W. Greiner, V. Grichine, A. Grossheim, S. Guatelli, P. Gumplinger, R. Hamatsu, K. Hashimoto, H. Hasui, A. Heikkinen, A. Howard, V. Ivanchenko, A. Johnson, F.W. Jones, J. Kallenbach, N. Kanaya, M. Kawabata, Y. Kawabata, M. Kawaguti, S. Kelner, P. Kent, A. Kimura, T. Kodama, R. Kokoulin, M. Kossov, H. Kurashige, E. Lamanna, T. Lampén, V. Lara, V. Lefebure, F. Lei, M. Liendl, W. Lockman, F. Longo, S. Magni, M. Maire, E. Medernach, K. Minamimoto, P. Mora de Freitas, Y. Morita, K. Murakami, M. Nagamatu, R. Nartallo, P. Nieminen, T. Nishimura, K. Ohtsubo, M. Okamura, S. O'Neale, Y. Oohata, K. Paech, J. Perl, A. Pfeiffer, M.G. Pia, F. Ranjard, A. Rybin, S. Sadilov, E. Di Salvo, G. Santin, T. Sasaki, N. Savvas, Y. Sawada, S. Scherer, S. Sei, V. Sirotenko, D. Smith, N. Starkov, H. Stoecker, J. Sulkimo, M. Takahata, S. Tanaka, E. Tcherniaev, E. Safai Tehrani, M. Tropeano, P. Truscott, H. Uno, L. Urban, P. Urban, M. Verderi, A. Walkden, W. Wander, H. Weber, J.P. Wellisch, T. Wenaus, D.C. Williams, D. Wright, T. Yamada, H. Yoshida, D. Zschiesche, G4 – a simulation toolkit, Nucl. Instr. Meth. A 506 (2003) 250–303.

[3] J. Allison, K. Amako, J. Apostolakis, H. Araujo, P.A. Dubois, M. Asai, G. Barrand, R. Capra, S. Chauvie, R. Chytracek, G.A.P. Cirrone, G. Cooperman, G. Cosmo, G. Cuttone, G.G. Daquino, M. Donszelmann, M. Dressel, G. Folger, F. Foppiano, J. Generowicz, V. Grichine, S. Guatelli, P. Gumplinger, A. Heikkinen, I. Hrivnacova, A. Howard, S. Incerti, V. Ivanchenko, T. Johnson, F. Jones, T. Koi, R. Kokoulin, M. Kossov, H. Kurashige, V. Lara, S. Larsson, F. Lei, O. Link, F. Longo, M. Maire, A. Mantero, B. Mascialino, I. McLaren, P.M. Lorenzo, K. Minamimoto, K. Murakami, P. Nieminen, L. Pandola, S. Parlati, L. Peralta, J. Perl, A. Pfeiffer,

M.G. Pia, A. Ribon, P. Rodrigues, G. Russo, S. Sadilov, G. Santin, T. Sasaki, D. Smith, N. Starkov, S. Tanaka, E. Tcherniaev, B. Tome, A. Trindade, P. Truscott, L. Urban, M. Verderi, A. Walkden, J.P. Wellisch, D.C. Williams, D. Wright, H. Yoshida, Geant4 developments and applications, IEEE Trans. Nucl. Sci. 53 (2006) 270–278.

[4] S. Incerti, A. Ivanchenko, M. Karamitros, A. Mantero, P. Moretto, H.N. Tran, B. Mascialino, C. Champion, V.N. Ivanchenko, M.A. Bernal, Z. Francis, C. Villagrasa, G. Baldacchino, P. Guèye, R. Capra, P. Nieminen, C. Zacharatou, Comparison of GEANT4 very low energy cross section models with experimental data in water, Med. Phys. 37 (2010) 4692.

[5] Z. Francis, S. Incerti, M. Karamitros, H.N. Tran, C. Villagrasa, Stopping power and ranges of electrons, protons and alpha particles in liquid water using the Geant4-DNA package, Nucl. Instr. Meth. B 269 (2011) 2307–2311.

[6] M. Karamitros, A. Mantero, S. Incerti, W. Friedland, G. Baldacchino, P. Barberet, M. Bernal, R. Capra, C. Champion, Z. El Bitar, Z. Francis, P. Guèye, A. Ivanchenko, V. Ivanchenko, H. Kurashige, B. Mascialino, P. Moretto, P. Nieminen, G. Santin, H. Seznec, H.N. Tran, C. Villagrasa, C. Zacharatou, Prog. Nucl. Sci. Technol. 2 (2011) 503–508.

[7] W. Friedland, M. Dingfelder, P. Kundrat, P. Jacob, Track structures, DNA targets and radiation effects in the biophysical Monte Carlo simulation code PARTRAC, Mutat. Res., Fundam. Mol. Mech. Mutagen. 711 (2011) 28–40.

[8] M.U. Bug, E. Gargioni, S. Guatelli, S. Incerti, H. Rabus, R. Schulte, A.B. Rosenfeld, Effect of a magnetic field on the track structure of low-energy electrons: a Monte Carlo study, Eur. Phys. J. D 60 (2010) 85–92.

[9] P. Lazarakis, M.U. Bug, E. Gargioni, S. Guatelli, H. Rabus, A.B. Rosenfeld, Comparison of nanodosimetric parameters of track structure calculated by the Monte Carlo codes Geant4-DNA and PTra, Phys. Med. Biol. 57 (2012) 1231–1250.

[10] M.A. Bernal, C.E. deAlmeida, C. Sampaio, S. Incerti, C. Champion, P. Nieminen, The invariance of the total direct DNA strand break yield, Med. Phys. 38 (2011) 4147–4153.

[11] Z. Francis, S. Incerti, V. Ivanchenko, C. Champion, M. Karamitros, M.A. Bernal, Z. El Bitar, Monte Carlo simulation of energy-deposit clustering for ions of the same LET in liquid water, Phys. Med. Biol. 57 (2012) 209–224.

[12] A. Mantero, H. Ben Abdelouahed, C. Champion, Z. El Bitar, Z. Francis, P. Guèye, S. Incerti, V. Ivanchenko, M. Maire, PIXE simulation in Geant4, X-Ray Spectrom. 40 (2011) 135–140.

[13] S. Incerti, H. Seznec, M. Simon, P. Barberet, C. Habchi, P. Moretto, Monte Carlo dosimetry for targeted irradiation of individual cells using a microbeam facility, Radiat. Prot. Dosim. 133 (2009) 2–11.

[14] D.E. Charlton, D.T. Goodhead, W.E. Wilson, H.G. Paretzke, The deposition of energy in small cylindrical targets by high LET radiations, Radiat. Prot. Dosim. 13 (1985) 123–125.

[15] D.E. Charlton, H. Nikjoo, J.L. Humm, Calculation of initial yields of single- and double-strand breaks in cell nuclei from electrons, protons and alpha particles, Int. J. Radiat. Biol. 56 (1989) 1–19.

[16] F.A. Cucinotta, H. Nikjoo, D.T. Goodhead, Model for radial dependence of frequency distributions for energy imparted in nanometer volumes from HZE particles, Radiat. Res. 153 (2000) 459–468.

[17] H. Nikjoo, D.T. Goodhead, D.E. Charlton, H.G. Paretzke, Energy deposition in small cylindrical targets by monoenergetic electrons, Int. J. Radiat. Biol. 60 (1991) 739–756.

[18] M.A. Bernal, J.A. Liendo, An investigation on the capabilities of the PENELOPE MC code in nanodosimetry, Med. Phys. 36 (2009) 620.

[19] P. Barberet, F. Vianna, M. Karamitros, T. Brun, N. Gordillo, P. Moretto, S. Incerti, H. Seznec, Monte-Carlo dosimetry on a realistic cell monolayer geometry exposed to alpha particles, Phys. Med. Biol. 57 (2012) 2189–2207.

[20] W. Friedland, P. Jacob, P. Bernhardt, H.G. Paretzke, M. Dingfelder, Simulation of DNA damage after proton irradiation, Radiat. Res. 159 (2003) 401–410.

[21] H. Nikjoo, L. Lindborg, RBE of low energy electrons and photons, Phys. Med. Biol. 55 (2010) R65–R109.

[22] J.W. Hooper, D.S. Harmer, D.W. Martin, E.W. McDaniel, Comparison of electron and proton ionization data with the born approximation predictions, Phys. Rev. 125 (1962) 2000–2004.

[23] H. Nikjoo, S. Uehara, Comparison of various Monte Carlo track structure codes for energetic electrons in gaseous and liquid water, Basic Life Sci. 63 (1994) 167–184.

[24] Z. Francis, S. Incerti, R. Capra, B. Mascialino, G. Montarou, V. Stepan, C. Villagrasa, Molecular scale track structure simulations in liquid water using the Geant4-DNA Monte-Carlo processes, Appl. Radiat. Isot. 69 (2011) 220–226.

[25] W. Friedland, H.G. Paretzke, F. Ballarini, A. Ottolenghi, G. Kreth, C. Cremer, First steps towards systems radiation biology studies concerned with DNA and chromosome structure within living cells, Radiat. Environ. Biophys. 47 (2008) 49–61.

[26] M. Bernal, C.E. deAlmeida, S. Incerti, C. Champion, V. Ivanchenko, The influence of the DNA structure on the total direct strand break yield. 2013, in preparation.

[27] C. Leloup, G. Garty, G. Assaf, A. Cristovão, A. Breskin, R. Chechik, S. Shchemelinin, T. Paz-Elizur, Z. Livneh, R.W. Schulte, V. Bashkirov, J.R. Milligan, B. Grosswendt, Evaluation of lesion clustering in irradiated plasmid DNA, Int. J. Radiat. Biol. 81 (2005) 41–54.

[28] M. Belli, R. Cherubini, M. Dalla Vecchia, V. Dini, G. Esposito, G. Moschini, O. Sapora, C. Signoretti, G. Simone, E. Sorrentino, M.A. Tabocchini, DNA fragmentation in mammalian cells exposed to various light ions, Adv. Space Res. 27 (2001) 393–399.

[29] D. Frankenberg, H.J. Brede, U.J. Schrewe, C. Steinmetz, M. Frankenberg-Schwager, G. Kasten, E. Pralle, Induction of DNA double-strand breaks by 1 H and 4 He Ions in primary human skin fibroblasts in the LET range of 8–124 keV/μm, Radiat. Res. 151 (1999) 540–549.